

A Numerical Study on the Dissolution Process of InGaSb under Zero Gravity

Xin JIN¹, Takuya YAMAMOTO¹, Youhei TAKAGI¹, Yasunori OKANO^{1,2,4,5}, Yuko INATOMI^{2,3,4},
Yasuhiro HAYAKAWA⁴ and Sadik DOST⁵

Abstract

In_xGa_{1-x}Sb bulk crystals have been grown on the International Space Station using a GaSb (feed) / InSb / GaSb (seed) sandwich-structured sample. In order to gain a deeper insight into the transport phenomenon and the relevant fundamental mechanisms during the dissolution process of InGaSb in this system, four numerical simulations with different temperature conditions and under the assumption of zero gravity were performed by the volume-averaging continuum model. Simulation results showed the heat loss through the bottom wall did not affect the final feed/seed dissolution lengths and the grown crystal interface shape. The final dissolution lengths of the feed and seed crystals were determined by the temperature calculated along the seed interface. The results also indicate that the actual temperature of the growth ampoule should be around 3K lower than that measured on the outside the protective cartridge.

Keyword(s): Crystal growth, InGaSb, Zero-gravity, Numerical simulation

Received 17 November 2016, Accepted 27 February 2017, Published 30 April 2017

1. Introduction

In_xGa_{1-x}Sb ternary semiconductor is a promising substrate material for applications such as optoelectronic and thermo-photovoltaic devices. Especially by adjusting its composition ratio, its lattice constant and wavelength can be varied from 6.09 ~ 6.48 Å and 1.70 ~ 6.88 μm¹⁾.

However, growing such high-quality homogeneous InGaSb crystals is very difficult on Earth due to gravity which gives rise to undesirable thermo-solutal convection in the melt, and segregation in the grown crystal that leads to compositional non-uniformity and consequently to poor crystal quality^{2,3)}.

However, the microgravity environment such as the International Space Station (ISS) can minimize all these adverse effects and allow the growth of high quality homogeneous crystals^{3,4)}. For this objective, a series of crystal growth experiments of In_xGa_{1-x}Sb have been carried out onboard the ISS to obtain a better understanding for the transport phenomena occurring during the dissolution and growth processes of InGaSb and the mechanisms controlling the dissolution lengths and the solution/solid interface shapes.

A vertical temperature gradient (top being hotter and bottom being cooler) method was adopted to grow the InGaSb single

crystals in a GaSb/InSb/GaSb sandwich-structured sample⁵⁾. Considering the different melting points of InSb (798.15 K) and GaSb (986.15 K), InSb melts first and then GaSb feed material (at the high-temperature region) dissolves into the InSb-melt (the dissolution process) and forms the In-Ga-Sb growth solution. Then the In-Ga-Sb solution reaches its supersaturation point, and the InGaSb crystal growth begins on the GaSb seed crystal at the bottom (at the lower-temperature region). This is the growth process.

Both experimental and numerical studies have been performed to have a better understanding of the dissolution and growth processes in the InGaSb system. For example, Dutta *et al.*²⁾ have shown that the forced convection in the melt could inhibit cracking of the crystal and improve the microscopic crystalline quality. Duffar *et al.*⁴⁾ have demonstrated that the InGaSb crystals grown in detached crucibles were found to have better structural qualities under microgravity. Hayakawa *et al.*³⁾ have found gravity has a significant effect on crystal compositions and solution-crystal interface shapes. Murakami *et al.*^{6,7)} have measured the growth rate of the crystal and found that the dissolution and growth processes were greatly affected by the gravity directions. Rajesh *et al.*^{5,8)} and Takagi *et al.*⁹⁾, both, have found out that under terrestrial

1 Department of Materials Engineering Science, Osaka University, 1-3 Machikaneyama, Toyonaka, Osaka 560-8531, Japan.

2 ISAS, Japan Aerospace Exploration Agency, 3-1-1 Yoshinodai, Chuo-ku, Sagamihara, Kanagawa 252-5210, Japan.

3 School of Physical Sciences, SOKENDAI, 3-1-1 Yoshinodai, Chuo-ku, Sagamihara, Kanagawa 252-5210, Japan.

4 Research Institute of Electronics, Shizuoka University, 3-5-1 Johoku, Naka-ku, Hamamatsu, Shizuoka 432-8011, Japan.

5 Crystal Growth Laboratory, University of Victoria, Victoria, BC V8W 3P6, Canada.

(E-mail: okano@cheng.es.osaka-u.ac.jp)

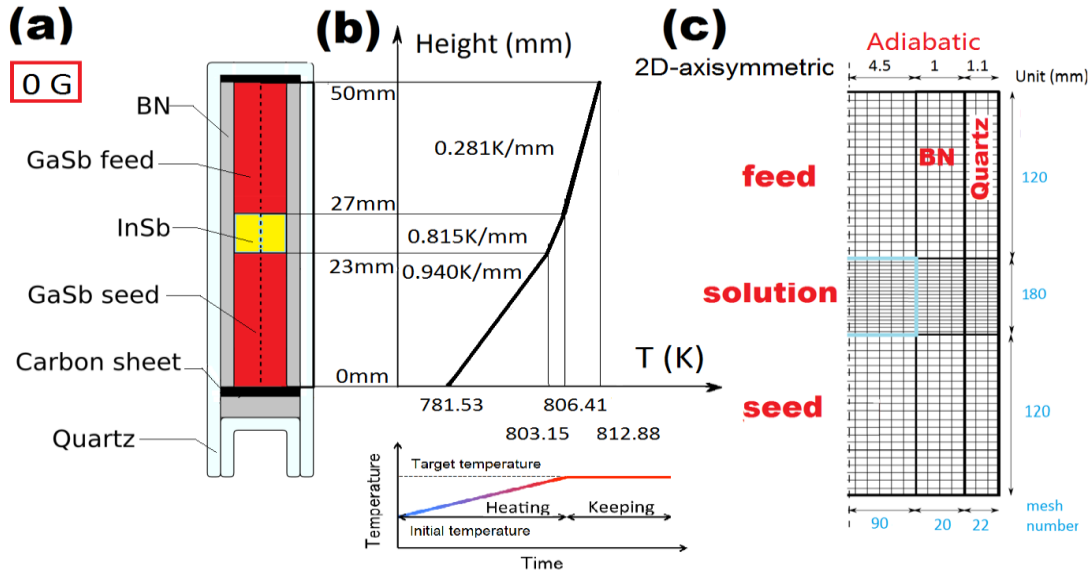


Fig. 1 Schematics of (a) the growth ampoule, (b) the applied temperature profile, and (c) the grid system of the simulation.

gravity the dissolution process is strongly influenced by thermo-solutal convection while under microgravity the dissolution process is diffusion dominant. Nobeoka *et al.*¹⁰ have shown that diffusion is dominant during the growth process under both normal and micro gravity. Mirsandi *et al.*¹¹ have demonstrated numerically that high interfacial kinetics which depends on crystal orientation can accelerate on the growth rate and feed (GaSb) dissolution. Inatomi *et al.*¹² have successfully studied the growth of InGaSb on the ISS and made comparisons with the terrestrial experiments. Recently Kumar *et al.*¹³ observed higher dissolution and growth rate in GaSb (111) B than (111) A.

In spite of these above-mentioned experimental and numerical studies, so far the mechanism determining the final dissolution lengths of the feed/seed crystals is still unclear^{8-11, 14}. All these simulation studies presented so far have not led to satisfactory results agreeing with those of experiments¹². For instance, they predicted either longer dissolution lengths for the seed crystal or a complete dissolution of the feed material¹⁴. To understand this issue, using the indium composition values in the experiments¹² and the phase diagram utilized in the numerical simulation²⁰, we calculated the temperature profile in the grown crystals. These calculated temperature values are lower than those used in the simulation¹⁴. We think that the reason for these discrepancies predicted in previous simulations is the use of temperature values obtained from the cartridge outside the growth ampoule during the constant-temperature period in the experiments (in space experiments the growth ampoule is placed in a protective cartridge). There would naturally be small temperature differences

between the growth ampoule and the outside cartridge¹⁵. Therefore, in order to examine the role of such small temperature differences in this sandwich system, in the present study we carried out four numerical simulations under the assumption of zero gravity with different temperature conditions.

2. Numerical Analysis

2.1 Numerical Model

A schematic description of the InGaSb crystal dissolution / growth system is shown in **Fig. 1**. The GaSb(feed)/InSb/GaSb(seed) sandwich sample was stacked in a quartz ampoule and sealed with Boron Nitride (BN) and carbon sheet as seen in **Fig. 1(a)**. The system was subjected to three vertical temperature gradients as shown in **Fig. 1(b)** with top being hotter and bottom being cooler. The whole system was heated at a heating rate of 0.001 K/s up to the target temperature and then kept constant.

To understand the dominant factors which determine the final

Table 1 Lower boundary conditions and heating settings.

Cases	Bottom wall temperature gradient (K/mm)	Heating time (s)	Target temperature (K)
A	0 (adiabatic)	6295.2	Original
B	1.00	6295.2	Original
C	1.00	6175.2	Original-3 K
D	1.00	5895.2	Original-10 K

dissolution length for the feed and seed crystals, we carried four numerical simulations with different temperature conditions as shown in **Table 1**. Case A adopted the previous experimental and numerical conditions¹⁴. Case B used the same heating settings during the heating period but adopted a new boundary condition for the bottom wall to investigate the effect of heat loss through the bottom wall in the dissolution process. In Case B, we changed the bottom wall condition from zero-gradient (adiabatic) to a fixed-gradient of 1.00 K/mm (As shown in **Fig. 1 (b)**, the temperature gradient between the seed interface and the bottom wall is 0.94 K/mm. However, for simplicity we used 1.00 K/mm gradient for the bottom wall in Case B). Also, since the interface temperatures calculated are higher than those of experiments, in Cases C and D we reduced the target temperatures for 3 K and 10 K by shortening the heating time to investigate the temperature difference between the growth ampoule and the outside cartridge (the growth ampoule has lower temperature compared to the outside cartridge)¹⁵.

2.2 Governing Equations

Physical properties of the In-Ga-Sb solution (L), GaSb (S), BN (BN), and quartz (Q) are given in **Table 2** (same as used previously¹⁶⁻¹⁸). The following assumptions were made in the present numerical simulation model:

(1) Densities of the solid and liquid phases are constant, and thus the associated volume changes during phase changes are negligible,

(2) Changes in physical properties (because of compositional variations) during the dissolution and growth processes are not

significant,

(3) In the beginning, the complete molten state of InSb was adopted (i.e., the initial GaSb concentration in the solution is zero).

The g-jitter effect (gravity fluctuation) on the ISS was not taken into account and the microgravity level was taken zero for simplicity. Under these assumptions, the governing equations of the crystal phase, namely the energy balance and mass transport equations are given as:

$$\frac{\partial T}{\partial t} = \alpha_i \nabla^2 T \quad (i = L, S) \quad (1)$$

$$\frac{\partial C}{\partial t} = D_i \nabla^2 C \quad (i = L, S) \quad (2)$$

where T is temperature, α_i is the thermal diffusivity of the crystal phases, and C and D are, respectively, the concentration and diffusion coefficient of GaSb.

In the solid phases (BN and Quartz), only the heat conduction equation was considered:

$$\frac{\partial T}{\partial t} = \alpha_i \nabla^2 T \quad (i = BN, Q) \quad (3)$$

where α_i is the thermal diffusivity of the solid phases.

In order to solve the above equations, we adopted the volume-averaging continuum model^{19,20}. In this model, the

Table 2 Physical properties used in the simulation.¹⁶⁻¹⁸

Properties	Symbol	Value
Liquid density	$\rho_L/(\text{kg}\cdot\text{m}^{-3})$	6300
Solid density	$\rho_S/(\text{kg}\cdot\text{m}^{-3})$	5600
BN density	$\rho_{BN}/(\text{kg}\cdot\text{m}^{-3})$	2280
Quartz density	$\rho_Q/(\text{kg}\cdot\text{m}^{-3})$	2200
Liquid thermal conductivity	$\lambda_L/(\text{W}\cdot\text{m}^{-1}\cdot\text{K}^{-1})$	17.0
Solid thermal conductivity	$\lambda_S/(\text{W}\cdot\text{m}^{-1}\cdot\text{K}^{-1})$	6.4
BN thermal conductivity	$\lambda_{BN}/(\text{W}\cdot\text{m}^{-1}\cdot\text{K}^{-1})$	54
Quartz thermal conductivity	$\lambda_Q/(\text{W}\cdot\text{m}^{-1}\cdot\text{K}^{-1})$	2.68
Liquid thermal diffusivity	$\alpha_L/(\text{m}\cdot\text{s}^{-2})$	9.0×10^{-6}
Solid thermal diffusivity	$\alpha_S/(\text{m}\cdot\text{s}^{-2})$	3.8×10^{-6}
BN thermal diffusivity	$\alpha_{BN}/(\text{m}\cdot\text{s}^{-2})$	8.2×10^{-6}
Quartz thermal diffusivity	$\alpha_Q/(\text{m}\cdot\text{s}^{-2})$	1.0×10^{-6}
Liquid specific heat	$c_{p,L}/(\text{J}\cdot\text{kg}^{-1}\cdot\text{K}^{-1})$	300
Solid specific heat	$c_{p,S}/(\text{J}\cdot\text{kg}^{-1}\cdot\text{K}^{-1})$	300
BN specific heat	$c_{p,BN}/(\text{J}\cdot\text{kg}^{-1}\cdot\text{K}^{-1})$	2900
Quartz specific heat	$c_{p,Q}/(\text{J}\cdot\text{kg}^{-1}\cdot\text{K}^{-1})$	1000
Liquid diffusion coefficient	$D_L/(\text{m}^2\cdot\text{s}^{-1})$	1.2×10^{-8}
Solid diffusion coefficient	$D_S/(\text{m}^2\cdot\text{s}^{-1})$	0
Latent heat	$La/(\text{J}\cdot\text{kg}^{-1})$	3.14×10^5

volume fractions of the solid and liquid phases are utilized. Based on temperature and concentration profiles and the phase diagram of the system, we can calculate the volume fractions of the solid and liquid phases and carry out the simulation. Relevant details on the numerical method and its relevant code validations can be found in our previous article²⁰.

2.3 Numerical Procedure

Figure 1(c) shows the two-dimensional axisymmetric grid system used in this simulation. The governing equations and the boundary conditions were discretized by the finite volume method. Simulations were carried out using the OpenFOAM package (a free open source CFD software package)²¹.

3. Results and discussion

Figure 2 shows the computed time evolution of the center of the seed interface for the four cases considered. The simulation in real time takes too long, thus, to accelerate it, we used a 25 times larger heating rate and a 25 times larger diffusion coefficient compared to the experimental values¹² in the dissolution process. Since the dissolution process is diffusion-dominant under zero gravity⁹, the use of a 25 times larger heating rate and a 25 times larger diffusion coefficient predicts almost same results for the dissolution length and interface shape (2.9 mm seed dissolution length, concave seed interface and feed complete dissolution when crystal growth began), as those of the simulation using the actual heating rate and diffusion coefficient values (2.8 mm seed dissolution length, concave seed interface and feed complete dissolution when crystal growth began). It can be seen from Fig. 2, firstly the solutes mainly dissolved from the hot feed crystal and diffused towards the cold seed interface and started to accumulate on the seed interface. Because of the low heating rate, the temperature in the beginning was really low and thus the crystal started to grow at the maximum height of 0.6 mm on the seed

interface. Then as the heating process continued, the temperature became higher and higher and the grown crystal on the seed dissolved again. When the solution reached its supersaturation point, growth started again on the seed and continued during the constant-temperature period. This process was the same in all four cases.

In addition, although we considered the same heating procedure (same target temperatures) in Cases A and B, even with or without heat loss through the bottom wall, there is no significant difference between two cases in terms of the final seed dissolution lengths and crystal growth time. In both cases, the growth process began around 6700 seconds and the final seed dissolution lengths were around 2.9 mm, where the experimental value is 2.3 mm¹².

In Cases B, C and D we used the same heat flux value on the bottom wall but different heating settings in the heating process. As seen, the dissolution processes are almost the same in all cases. However, when the heating time was shortened ($B > C > D$), in other words the target temperature values were smaller (B: original, C: original -3 K, D: original -10 K), the crystal growth started earlier and the final seed dissolution length became smaller (B: 2.9 mm, C: 2.1 mm, D: 1.0 mm). Among all these results, in terms of the seed final dissolution length, the prediction from Case C was the closest to that of the experiments¹².

Figure 3 shows the temperature along the center line (axis) when the crystal growth began in the constant temperature period for Cases A, B, C and D. Results showed that, by reducing the target temperature in the constant-temperature period (Cases C and D), the temperatures along the center line (axis) were accordingly reduced and thus the feed crystal was not dissolved completely in Cases C and D.

The temperature distribution of Case A is very similar to Cases B, C and D (except the region between the bottom wall and the seed interface). The heat loss through the bottom wall in Cases B, C and D only affected the temperature distribution in the seed

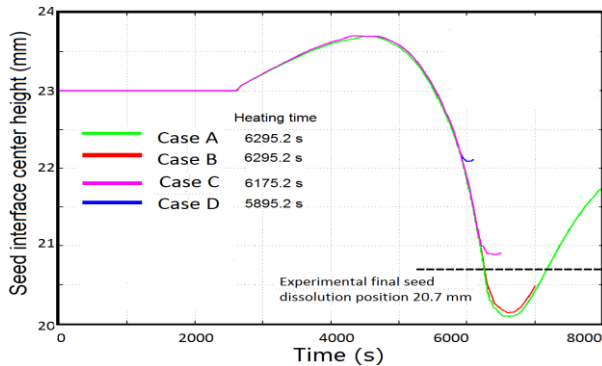


Fig. 2 Time evolution of the centre of the seed interface in the dissolution process.

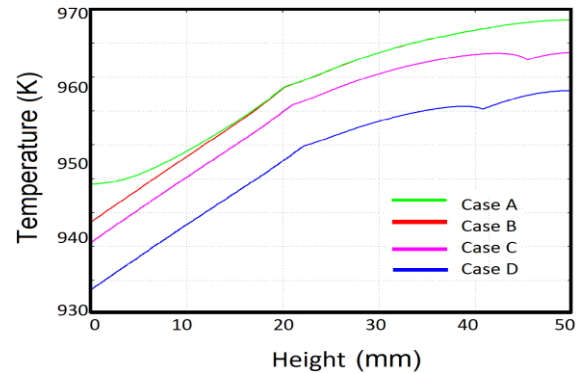


Fig. 3 Temperature variation along the center line (axis) at the onset of crystal growth.

crystal/solid region, making the axial temperature lower than in the adiabatic cases (Case A). However, the heat loss through the bottom wall has no effect on the final dissolution lengths.

Figure 4 shows the computed temperature distribution in the whole ampoule, the concentration profile of the crystal at the onset of crystal growth in Cases A, B, C and D. As for the temperature distribution in Cases A and B, not only the maximum and

minimum temperatures for the whole cartridge are the same, but also the temperature distribution patterns are very similar. Except for the lower region near the bottom wall, the temperature distribution is almost the same everywhere including the region around the grown crystal. In the lower region around the bottom wall, as seen from the figure, in Case A (the adiabatic boundary condition), the heat flux is through the top corner (the hottest

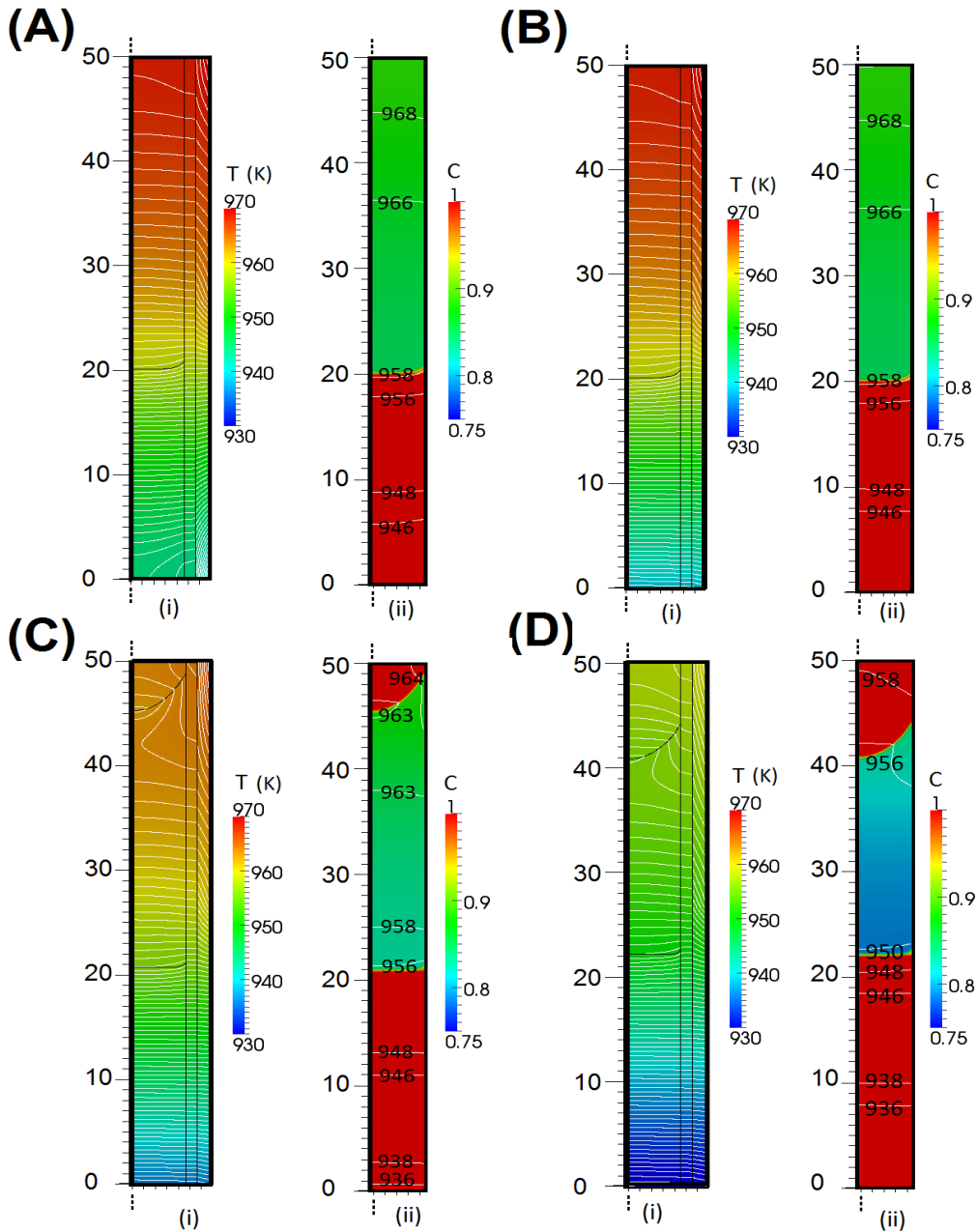


Fig. 4 Computed temperature (i) and Ga concentration (ii) distributions at the onset of crystal growth.

point) and heat loss is through the bottom corner (the coolest point). In Case B (the fixed-gradient boundary condition 1.00 K/mm), since there is a temperature gradient along the bottom wall, the heat penetrated from the top corner goes out directly through the bottom wall (the horizontal isothermal lines).

In addition, **Fig. 4 (ii)** shows the concentration profiles for Cases A and Case B. When the crystal growth began on the seed, in both cases the feed crystal dissolved completely. The interface shape and dissolution length for the seed in Case A are the same as those in Case B because the temperature distribution around the seed in both Cases A and B are similar. As also seen from **Fig. 4 (ii)**, the concentration profile and isothermal lines (956, 958, 966, 968 K) in the solution are the same for Cases A and B. In the lower region near the bottom wall, the isothermal lines for 946 K and 948 K are different. Since these temperature differences are in the seed/solid region, there is no significant effect on the dissolution process in these two cases.

Figure 4 also shows the computed temperature distribution for the whole ampoule and the concentration of the crystal at the onset of crystal growth in Cases C and D. Cases C and D have the same boundary condition as Case B (fixed gradient 1.00 K/mm for the bottom wall) but with the reduced target temperature of the whole ampoule by 3 K and 10 K. As shown in **Fig. 4(i)**, in both cases the heat flows from the top corner (the hottest point) and gets out through the bottom wall similar to Case B. However, in Cases C and D with decreased temperatures (by 3 K and 10 K compared to Case B), the computed temperature distributions are very different from the previous Case B, especially in the upper region between the top wall and the feed crystal interface. Unlike Case B, in Cases C and D due to reduced temperatures, the feed did not dissolve completely at the onset of growth (which agrees with the experimental results). Meanwhile the temperature distribution profile in the lower region between the seed interface and the bottom wall in Cases of B, C, and D are almost the same, except the isothermal lines values (958 K, 956 K, 950 K). Based on these temperature distributions, the seed interface shape in all these three cases is concave towards the bottom. In addition, as seen in **Fig. 2** due to the reduced target temperatures, the dissolution process ended earlier, and the crystal growth also began earlier. Finally, the final seed dissolution lengths predicted are 2.9 mm in Case B, 2.1 mm in Case C and 1.0 mm in Case D, as compared with the experimental values of 2.3 mm¹²⁾. This implies that the actual case is somewhere between Case B and Case C.

In terms of the concentration profile of the crystal at the onset of growth, by comparing the concentration profiles of Cases B, C,

and D, we see that (with decreased temperatures), the minimum Ga concentration in the solution consequently decreased: from 0.847 in Case B to 0.828 in Case C, and to 0.787 in Case D. At the same time the temperature along the seed interface became 958K in Case B, 956 K in Case C, and 950 K in Case D. Also according to the phase diagram used in our numerical simulation²⁰⁾, when the temperature along the seed interface was lower, the equilibrium Ga concentration in the solution became smaller. This means that in the case with lower target temperature, less material was dissolved from the feed.

Results of four cases are tabulated in **Table 3** for comparison. Case C predicts the closest dissolution length value (2.1 mm) compared with that of the experiment¹²⁾ (2.3 mm), and with some undissolved feed crystals being left. Thus, Case C was taken as an example and its interface positions at the center and periphery points for the feed and seed crystals are shown in **Fig. 5**.

Table 3 Summary of results.

Label	A	B	C	D
Crystal growth time (s)	6670	6700	6410	6050
Feed center dissolution length (mm)	All	All	18.4	13.7
Seed center dissolution length (mm)	2.9	2.9	2.1	1.0
Minimum solution concentration	0.848	0.847	0.828	0.787

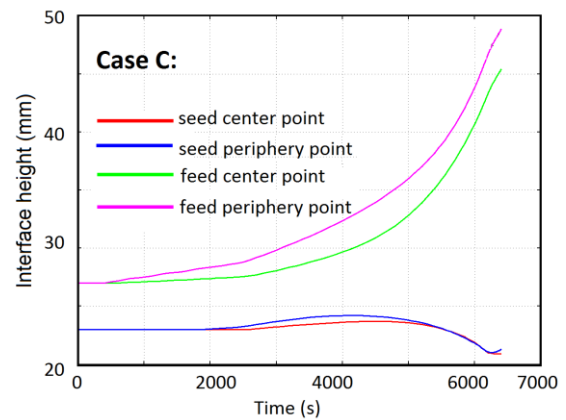


Fig. 5 Interface positions at the center and periphery points in Case C in the dissolution process.

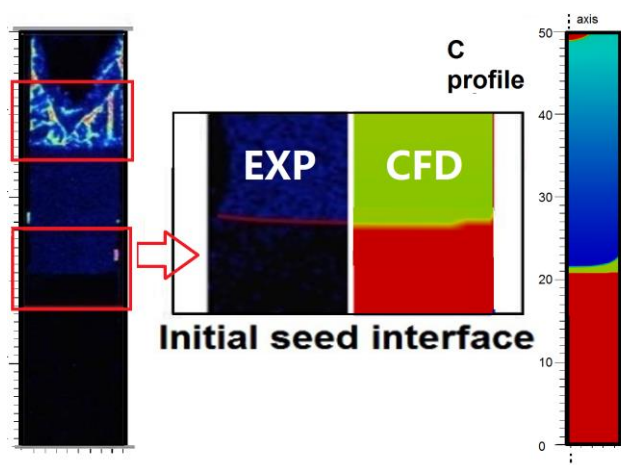


Fig. 6 Comparison of concentration profiles of Case C and the experimental (electron probe micro analysis)¹²⁾.

Simulations showed that the center of the feed dissolves slower than its periphery. This is because temperature is higher at the same height in the periphery than the center (this is the case for both heating processes, i.e. the one with increasing temperature and the one with constant temperature).

Simulation also predicts that, in the constant-temperature period, since the temperature is higher at the center of the seed than its periphery, the final growth of InGaSb crystals first starts from the periphery and then from the center. This prediction is in a good agreement with the experimental results¹²⁾.

Fig. 6 presents the comparison between Case C and experimental results¹²⁾. Both the interface shapes and the seed final dissolution lengths are in good agreement with those of the experiment.

4. Conclusion

Two-dimensional asymmetrical numerical simulation of InGaSb crystal growth (using the experimental size) was successfully performed under zero-gravity for four different heating conditions. The following conclusions can be drawn.

(1) In Cases A and B, simulations predict that the heat loss through the bottom wall did not have a significant effect on the final dissolution lengths for the seed and feed crystals. Even though the temperature distribution in the seed crystal (solid) was changed due to the bottom boundary condition, the temperature profiles along the seed crystal and the In-Ga-Sb solution were not changed.

(2) In Cases B, C and D, we predict that the final dissolution

lengths for the seed and feed crystals are determined by temperature conditions especially in the region around the seed interface. And the temperature difference between inside the growth sample ampoule and outside the protective cartridge cannot be ignored.

The present numerical simulation predicted more dissolution for the feed crystal than that of the experiments. This may be attributed to the additional heat loss from the top wall due to radiation. We plan in our future work to investigate the effect of heat loss through the top wall on the dissolution length of the feed crystal.

References

- 1) G. Dhanaraj, K. Byrappa, V. Prasad and M. Dudley: Springer handbook of crystal growth. Springer, 2010.
- 2) P.S. Dutta and A.G. Ostrogorsky: J. Appl. Phys., **194** (1998) 1.
- 3) Y. Hayakawa, Y. Okano, A. Hirata, N. Imaishi, Y. Kumagiri, X. Zhong, X. Xie, B. Yuan, F. Wu, H. Liu, T. Yamaguchi, and M. Kumagawa: J. Cryst. Growth, **213** (2000) 40.
- 4) T. Duffar, M.D. Serrano, C.D. Moore, J. Camassel, S. Contreras, P. Dusserre, A. Rivoallant and B.K. Tanner: J. Cryst. Growth, **192** (1998) 63.
- 5) G. Rajesh, M. Arivanandhan, H. Morii, T. Aoki, T. Koyama, Y. Momose, A. Tanaka, T. Ozawa, Y. Inatomi, and Y. Hayakawa: J. Cryst. Growth, **312** (2010) 2677.
- 6) N. Murakami, K. Arafune, T. Koyama, M. Kumagawa and Y. Hayakawa: J. Cryst. Growth, **263** (2004) 320.
- 7) N. Murakami, K. Arafune, T. Koyama, M. Kumagawa and Y. Hayakawa: J. Cryst. Growth, **275** (2005) 433.
- 8) G. Rajesh, M. Arivanandhan, N. Suzuki, A. Tanaka, H. Morii, T. Aoki, T. Koyama, Y. Momose, T. Ozawa, Y. Inatomi, Y. Takagi, Y. Okano and Y. Hayakawa: J. Cryst. Growth, **324**, (2011) 157.
- 9) Y. Takagi, N. Suzuki, Y. Okano, A. Tanaka, Y. Hayakawa and S. Dost: Trans. JSASS Aerospace Tech. Japan, **10** (2012) Ph_1.
- 10) M. Nobeoka, Y. Takagi, Y. Okano, Y. Hayakawa and S. Dost: J. Cryst. Growth, **385** (2014) 66.
- 11) H. Mirsandi, T. Yamamoto, Y. Takagi, Y. Okano, Y. Inatomi, Y. Hayakawa and S. Dost: Microgravity Sci. Technol., **27** (2015) 313.
- 12) Y. Inatomi, K. Sakata, M. Arivanandhan, G. Rajesh, V. Nirmal Kumar, T. Koyama, T. Ozawa, Y. Okano and Y. Hayakawa: npj Microgravity, **1** (2015) 15011.
- 13) V. Nirmal Kumar, M. Arivanandhan, G. Rajesh, T. Koyama, Y. Momose, K. Sakata, T. Ozawa, Y. Okano, Y. Inatomi, and Y. Hayakawa: npj Microgravity, **2** (2016) 16026.
- 14) X. Jin, H. Mirsandi, T. Yamamoto, Y. Takagi, Y. Okano, Y. Inatomi, Y. Hayakawa and S. Dost: JJAP Conf. Proc., **4** (2016) 011107.
- 15) Y. Inatomi, K. Sakata, M. Arivanandhan, G. Rajesh, Y. Hayakawa, A. Tanaka, T. Ozawa, Y. Okano, T. Ishikawa, M. Takanagi, S. Yoda and Y. Yoshimura: Tran. JSASS Aerospace Tech. Japan, **28** (2012) ph_1.
- 16) Y. Sato, T. Nishizuka, T. Takamizawa, T. Yamamura and Y. Waseda: Int. J. Thermophysics, **23** (2002) 235.
- 17) C. Stelian, T. Duffar and I. Nicoara: J. Cryst. Growth, **255** (2003) 40.
- 18) K. Abe, S. Sumioka, K.-I. Sugioka, M. Kubo, T. Tsukada, K. Kinoshita, Y. Arai and Y. Inatomi: J. Cryst. Growth, **402** (2014) 71.
- 19) C. Beckermann and R. Viskanta: Physicochem. Hydrodyn., **10** (1988) 195.
- 20) T. Yamamoto, H. Mirsandi, X. Jin, Y. Takagi, Y. Okano, Y. Inatomi, Y. Hayakawa and S. Dost: Numer. Heat Tr. B-fund., **70** (2016) 441.
- 21) See <http://www.openfoam.com> for the open source CFD toolbox, OpenFOAM.